Space-time monitoring of seafloor velocity changes using seismic ambient noise

Peng Guo[1,2], Erdinc Saygin[1,2] and Brian Kennett[3]

[1]Deep Earth Imaging Future Science Platform, The Commonwealth Scientific and Industrial Research Organisation (CSIRO), Kensington, Western Australia 6151, Australia

[2]Energy, The Commonwealth Scientific and Industrial Research Organisation (CSIRO), Kensington, Western Australia 6151, Australia

[3]Research School of Earth Sciences, The Australian National University, Canberra, Australian Capital Territory 2601, Australia

Key Points:

- We present a new method for space-time monitoring of subsurface velocity changes in the horizontal and depth domain using seismic ambient noise.
- We compute time-lapse images of seafloor seismic velocity and observe shear-wave velocity changes up to 0.8%.
- The method opens new avenues for 4-D subsurface monitoring using dense passive seismic arrays.

Corresponding author: Peng Guo, `peng.guo@csiro.au; pengguo.geos@gmail.com`

Abstract

We use seismic ambient noise recorded by dense ocean bottom nodes (OBNs) in the Gorgon gas field, Western Australia, to compute time-lapse seafloor models of shear-wave velocity. The extracted hourly cross-correlation (CC) functions in the frequency band $0.1 - 1$ Hz contain mainly Scholte waves with very high signal to noise ratio. We observe temporal velocity variations (dv/v) at the order of 0.1% with a peak velocity change of 0.8% averaged from all station pairs, from the conventional time-lapse analysis with the assumption of a spatially homogeneous dv/v. With a high-resolution reference (baseline) model from full waveform inversion of Scholte waves, we present an elastic wave equation based double-difference inversion (EW-DD) method, using arrival time differences between the reference and time-lapsed Scholte waves, for mapping temporally varying dv/v in the heterogeneous subsurface. The time-lapse velocity models reveal increasing/decreasing patterns of shear-wave velocity in agreement with those from the conventional analysis. The velocity variation exhibits a ∼24-hour cycling pattern, which appears to be inversely correlated with sea level height, possibly associated with dilatant effects for porous, low-velocity shallow seafloor and rising pore pressure with higher sea level. This study demonstrates the feasibility of using dense passive seismic surveys for quantitative monitoring of subsurface property changes in the horizontal and depth domain.

Plain Language Summary

Unlike seismic waves generated by earthquakes or human-made sources, seismic ambient noise is the ubiquitous background vibration of the solid Earth recorded by seismic sensors, mainly due to the interaction of ocean waves and the seafloor. We extract virtual Scholte waves travelling along the interface between the ocean and the seafloor, using seismic interferometry on an hourly basis, from the seafloor ambient noise recorded by dense ocean bottom nodes. Conventional passive monitoring techniques assume a spatially homogeneous relative velocity changes. With this assumption, the waveform differences on the extracted Scholte waves reveal temporal variations in the velocity of shear waves up to 0.8%. The velocity variation in this study exhibits a ∼24-hour cycling pattern, which seems inversely correlated with sea level height, possibly associated with dilatant effects for porous, low-velocity shallow seafloor and rising pore pressure with high sea level. Furthermore, we push the limits of passive monitoring with advanced wave-equation based inversion technique enabling mapping the velocity change into detailed spatial distribution. Therefore we not only infer how velocity changes in time but also provide insights on where the velocity changes occur in 3-D beneath the seabed.

1 Introduction

Seismic ambient noise (passive seismic data) is an ubiquitous background vibration of the solid Earth recorded by seismic sensors (Longuet-Higgins, 1950; Nishida, 2013; Ardhuin et al., 2015). The primary sources of seismic ambient noise are loads on the Earth's surface from pressure perturbations in the ocean and the atmosphere (Stehly et al., 2006; Gualtieri et al., 2020). Besides the low-frequency Earth's hum with periods longer than 30 s (Ardhuin et al., 2015), seismic ambient noise contains mainly primary (10 - 20 s) and secondary (5 - 10 s) microseisms. The primary mechanism comes from the direct coupling between the ocean waves and the solid Earth, with a period similar to that of the main ocean swell (Hasselmann, 1963). The secondary mechanism comes from the nonlinear interaction between direct swells and those reflected at the coast (Longuet-Higgins, 1950; Lindsey et al., 2019). A cross-correlation (CC) of the ambient noise wavefield recorded at two receivers provides an estimate of the emprical interstation Green's function, which can be interpreted as the seismic response that would be measured at one of the receiver locations as if there is a source at the other location (Campillo & Paul, 2003; Shapiro & Campillo, 2004; Roux et al., 2005; Larose et al., 2006; Bensen et al., 2007; Saygin &

Kennett, 2012; Nakata et al., 2016). The dominant signals extracted from seismic ambient noise are usually surface waves (e.g. Shapiro & Campillo, 2004; Stehly et al., 2006; Brenguier et al., 2016; Chen & Saygin, 2022), though body waves have also been observed in favourable circumstances (e.g. Roux et al., 2005; Nakata et al., 2016; Saygin et al., 2017; Castellanos et al., 2020).

Temporal variations of subsurface physical properties have been often observed; for example, from environmental changes (Sens-Schönfelder & Wegler, 2006; Takano et al., 2014, 2019; Hillers et al., 2015; Clements & Denolle, 2018; Mao et al., 2022; Kramer et al., 2023; S. Zhang et al., 2023) and within zones of active tectonic activities such as volcanos and faults (Poupinet et al., 1984; Wegler et al., 2006; Brenguier et al., 2008; Minato et al., 2012; Brenguier et al., 2016; Viens et al., 2018; Barreyre et al., 2022; Tonegawa et al., 2023), natural resources (e.g., hydrocarbon, geothermal) production fields (Batzle & Wang, 1992; Lumley, 2001; Obermann et al., 2015; Sánchez-Pastor et al., 2019), and carbon/hydrogen underground storage in subsurface rock formations (Arts et al., 2004; Lumley, 2010; Zhu et al., 2019; Ringrose et al., 2021; Krevor et al., 2023). The relative change in the speed of seismic waves (dv/v) has been widely used as a proxy for the changes of in-situ subsurface rock physical properties. In recent years it has been demonstrated that subsurface monitoring using seismic ambient noise is a powerful and cost-effective solution for detecting and quantifying the time-lapse dv/v (Sens-Schönfelder & Wegler, 2006; Brenguier et al., 2014; Hillers et al., 2015; Obermann et al., 2015; Clements & Denolle, 2018; Sánchez-Pastor et al., 2019; Takano et al., 2019; Brenguier et al., 2020; Mao et al., 2022; Tonegawa et al., 2023). The ever-present natural ambient sources enable continuous and reliable estimates of interstation seismic responses for pairs of seismic stations across time, for example at a daily (Hadziioannou et al., 2011; Minato et al., 2012; de Ridder & Biondi, 2013; Brenguier et al., 2020) or hourly basis (Mao et al., 2019; Oakley et al., 2021; Kramer et al., 2023; Takano & Nishida, 2023). The waveform changes (e.g., the travel time shifts) between the reference and time-lapse CC functions can be used for estimating dv/v (Sens-Schönfelder & Wegler, 2006; Clarke et al., 2011; Richter et al., 2014; Lecocq et al., 2014). Compared with expensive controlled-source seismic surveys for time-lapse monitoring (Lumley, 2001; Hicks et al., 2016), seismic monitoring using ambient noise helps reduce the operational cost significantly, is environmentally friendly and can be more readily embraced by the community. Passive monitoring is also preferred over subsurface monitoring methods that rely on naturally occurred earthquakes, because the latter lacks repeatability and universal distribution (Kamei & Lumley, 2017).

The extracted emprical interstation seismic responses contain the direct (ballistic) and multi-scattered coda waves. Both have been used for monitoring temporal variability of subsurface velocities (Snieder et al., 2002; Sens-Schönfelder & Wegler, 2006; Takano et al., 2020; Fokker et al., 2023). It is common practice for seismic passive monitoring to detect the temporal changes with an assumption of spatially homogeneous change (Snieder et al., 2002; Sens-Schönfelder & Wegler, 2006). However, it remains challenging to map or localize the detailed spatial distribution. There have been studies using direct arrivals of surface waves (de Ridder & Biondi, 2013; de Ridder et al., 2014; Mordret et al., 2014) that localize the velocity changes in the horizontal plane, and use the eikonal equation to describe the physics, which is less accurate than inversion methods based on the full elastic-wave equations. Mordret et al. (2020) estimated velocity velocity changes in depth from dispersion measurements using a 1-D assumption. For multiply scattered coda waves, the spatial extent of the velocity changes can be determined from travel-time shifts using the coda-wave sensitivity kernels, which describe wave propagation by delineating the likelihood of travel path in a statistically characterized scattering media (Pacheco & Snieder, 2005; Obermann, Planès, et al., 2013; Obermann, Schimmel, et al., 2013; Margerin et al., 2016; Sánchez-Pastor et al., 2018; Rodríguez Tribaldos & Ajo-Franklin, 2021; Mao et al., 2022, 2023). Coda waves allow the detection of subtle velocity changes on the order of 0.01% (Sens-Schönfelder & Wegler, 2006; Mao et al., 2019), but the spatial resolution is relatively low. Compared with the established workflows for determining quantitative 4-D (space-time) models of temporal velocity changes using body waves from controlled seismic sources (e.g. Lumley, 2001, 2010; Z. Zhang & Huang, 2013; Yang et al., 2016; Hicks et al., 2016; Ringrose et al., 2021), there has been a significant knowledge gap for subsurface space-time monitoring using surface waves from ambient noise.

We present a pilot study for space-time monitoring of subsurface physical property changes using ocean bottom ambient noise data, which not only enables the detection of temporal average changes but also provides insights into their spatial distribution. We extract Scholte waves in the frequency band 0.1 – 1 Hz on an hourly basis from two-day seafloor seismic noise recorded by a dense array of ocean bottom nodes (OBNs). Time-lapse analysis shows temporal changes of the seafloor velocity up to ∼0.8%. With a seafloor model from full waveform inversion (FWI) of reference Scholte waves, we propose an elastic wave equation based double-difference inversion (EW-DD) method using differential wave arrival times for mapping time-lapse velocity changes in space. Synthetic and field data applications show that it is feasible to perform space-time subsurface monitoring using ambient noise, i.e., detecting and localizing subtle subsurface velocity changes using ambient noise data from dense seismic arrays.

2 Data and Ambient Noise Interferometry

Between November 2015 and April 2016, Chevron Australia and its partners acquired a three-dimensional (3-D) seismic survey using active-source ocean bottom nodes (OBNs) over the Gorgon gas field for a better description of the Gorgon reservoir sands for carbon capture and storage. The survey area is located on the North West Shelf offshore of Western Australia, approximately 200 km from the mainland (Figure 1a and 1b). Both the in-line and cross-line intervals were 375 m, with 120 OBN lines covering an area of ∼436 km^2. The inline direction was 115^o/295^o, about perpendicular to the coastal line. The water depth in the survey region was between 200 and 600 m. The survey contains 3099 seismic nodes, which were deployed from the north to the south and gradually covered the whole area of the Gorgon field with a rolling phase deployment (Chen & Saygin, 2022). At the peak of the survey, over 1,000 nodes were recording simultaneously. Each node comprised four channels, with two horizontal components (X, Y) and one vertical component (Z) for measuring displacement, and a hydrophone component for recording pressure. The data were recorded continuously with a 2 millisecond interval. The survey used controlled air-gun seismic sources, but there were several quiet time windows without using controlled active sources, for example, during public holidays. Clock drift has been corrected during data preprocessing (Rentsch et al., 2023). The recorded ambient seismic wavefield in the absence of active seismic sources provides the opportunity for passive subsurface monitoring using a dense seismic array of industrial scale. We select a time window around the New Year's holiday, Julian Days 1 and 2 of 2016, for the passive seismic monitoring experiment.

We detrend and down-sample the vertical component of the data from 250 Hz to 20 Hz with anti-aliasing filtering. The ambient noise data are then filtered to the frequency band 0.1 – 1 Hz. We divide the recordings of the selected quiet time window without active source shooting into hour-long segments; each segment is then subdivided into 45 s long records with a 50% overlap. We calculate CC functions for each time window of ambient noise recordings for all the station pairs, and use the phase-weighted stacking (Schimmel et al., 2011) within each hour-long segment to improve the signal to noise ratio. Figure 1c shows the CC functions at Hour 15 Day 1 for Line 3924 (in-line direction, indicated by the black arrow in Figure 1b), which contain mainly Scholte waves (travelling along the interface between the ocean and the seafloor) and provide constraints on the shear-wave velocity of the seafloor. This is consistent with the observation that interface waves, for example Rayleigh waves for the air-solid interface or Scholte waves for the fluid-solid interface, dominate the vertical component of the microseism records

(Gualtieri et al., 2020). The extracted hourly CC functions have a very high signal to noise ratio. The energy concentrates on the positive side of the CC time lags and the empirical Scholete waves are barely visible in the acausal side, suggesting that most of the ambient noise between 0.1 and 1 Hz propagates from the coast to the ocean in this particular scenario.

3 Methods and results

3.1 Temporal monitoring of seismic velocity

For each station pair, reference (baseline) data can be obtained by stacking the repetitive estimates of CC functions for that pair across all the available hours from the two-day passive noise data recordings. We compare the causal part of the direct Scholte wave arrivals of the reference data with that of the hourly CC functions (monitoring data) to quantify the velocity variations in time (dv/v). We apply Moving-Window Cross-Spectral Analysis (Poupinet et al., 1984; Clarke et al., 2011) to the Scholte waves, with the assumption that dv/v is homogeneous in space. Figures 2a and 2b depict the derived velocity changes from two selected station pairs. Figure 2c shows the velocity changes from all the station pairs, along with the corresponding average changes across the entire two-day monitoring period. We observe seafloor velocity changes up to 0.8% (Figure 2c), exhibiting a probable sinusoidal pattern with a cycle close to 24 hours. The velocity changes in Figure 2 can be interpreted as the average velocity perturbation of the subsurface medium through which the Scholte waves propagate. The temporal changes of velocities from more survey lines, as indicated by the black arrows in Figure S1, are shown in Figure S2, suggesting similar patterns of velocity changes in line with Figure 2.

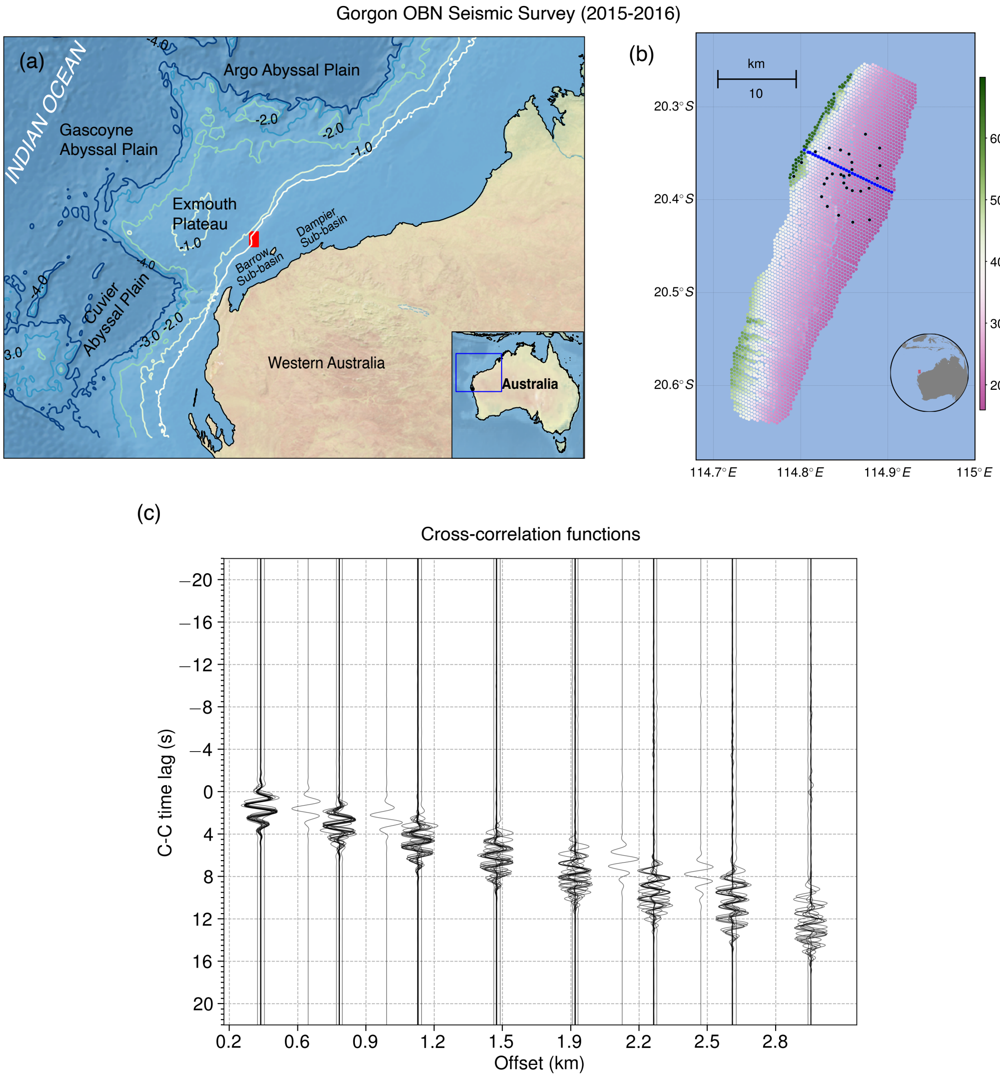

Figure 1. Map of the ocean bottom seismic survey in Western Australia and cross-correlation (CC) functions from ambient noise interferometry. (a) Ocean Bottom Node (OBN) seismic survey in the Gorgon gas field offshore Western Australia by Chevron Australia and its partners. (b) Zoom-in of the red rectangle in (a). Each dot refers to an OBN with the color suggesting water depth. The line of node with the blue color indicates Line 3924 used in the study. The OBNs on the three spiral arms in the black color are used for beamforming analyis of mapping ambient noise sources. (c) CC functions for Line 3924 sorted by offsets (the distance between a station pair) from Hour 15 of Julian Day 1, 2016. We limit the CC functions to 3 km offset.

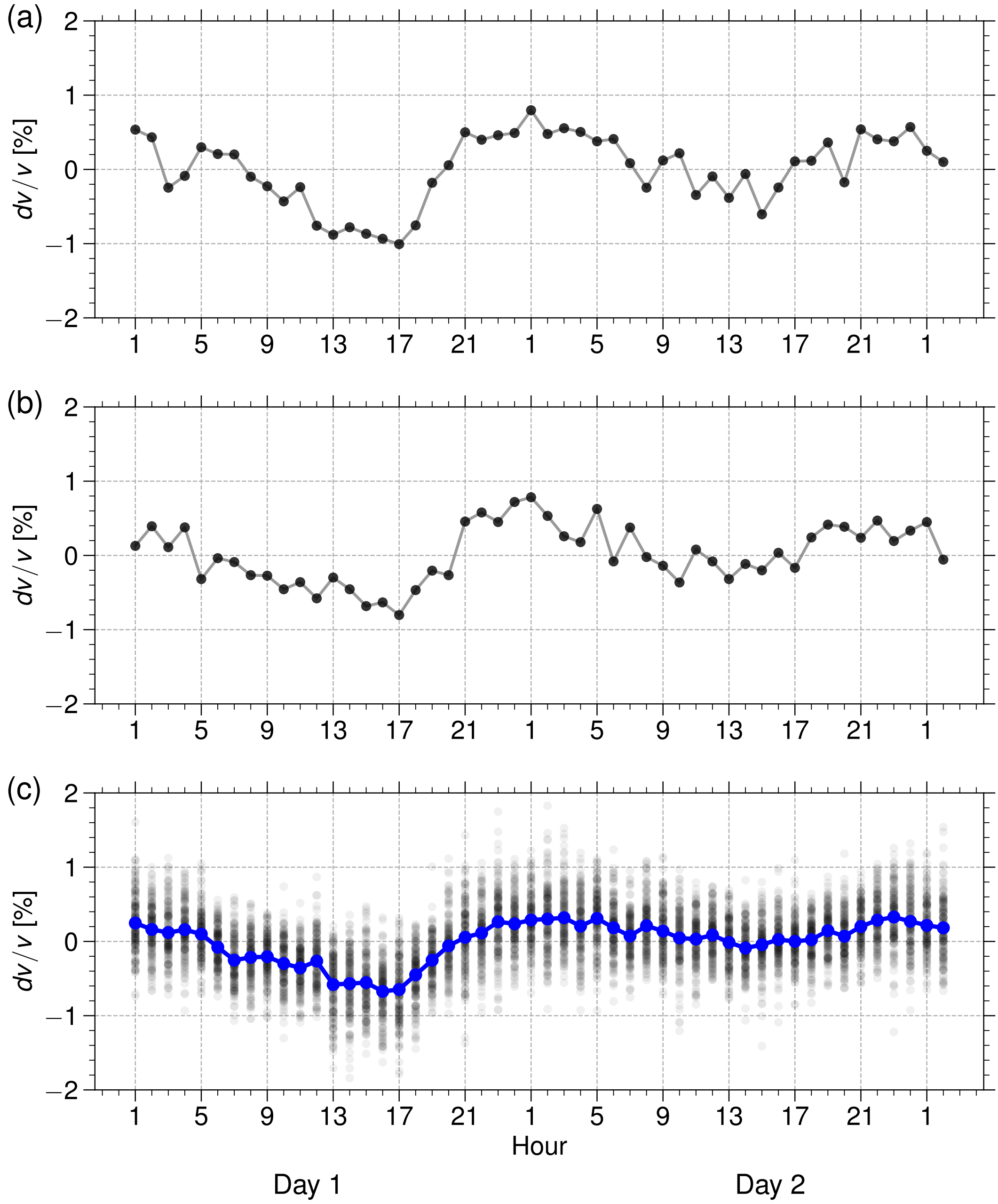

Figure 2. The relative seismic velocity changes (dv/v) in time during the passive monitoring period of Julian Day 1 and 2, 2016. The velocity changes are estimated from the direct arrivals of Scholte waves in the CC functions of station pairs in Line 3924 (Figure 1). (a) and (b) depict the dv/v from two station pairs, with station distances of 1.2 km and 2.4 km. (c) shows the velocity changes from all the station pairs (with a maximum offset 3.2 km) in Line 3924. Each black dot is the dv/v from a station pair measurement. The blue curve in (c) is the average dv/v.

We sort the CC functions of all the station pairs into common-station gathers. Each common-station gather can be considered as a seismic common-source gather so that the shared common station is the virtual source for generating seismic waves, and the rest of the stations from the selected survey line are the receivers. Figure 3 contains common-station gathers of the reference data and the monitoring data from Hour 15 of Day 1 (Figure 3a) and Hour 1 of Day 2 (Figure 3b). We observe that the main difference between the reference and monitoring data of different hours is in the arrival times of the Scholte waves. Scholte waves from Hour 15 of Day 1 arrive later than the reference data (Figures 3a and 3c), indicating a velocity decrease than the reference model, while those from Hour 1 of Day 2 arrive at an earlier time than the reference data (Figures 3b and 3d), suggesting a velocity increase. The observations from the common-station gathers are consistent with the velocity changes in Figure 2.

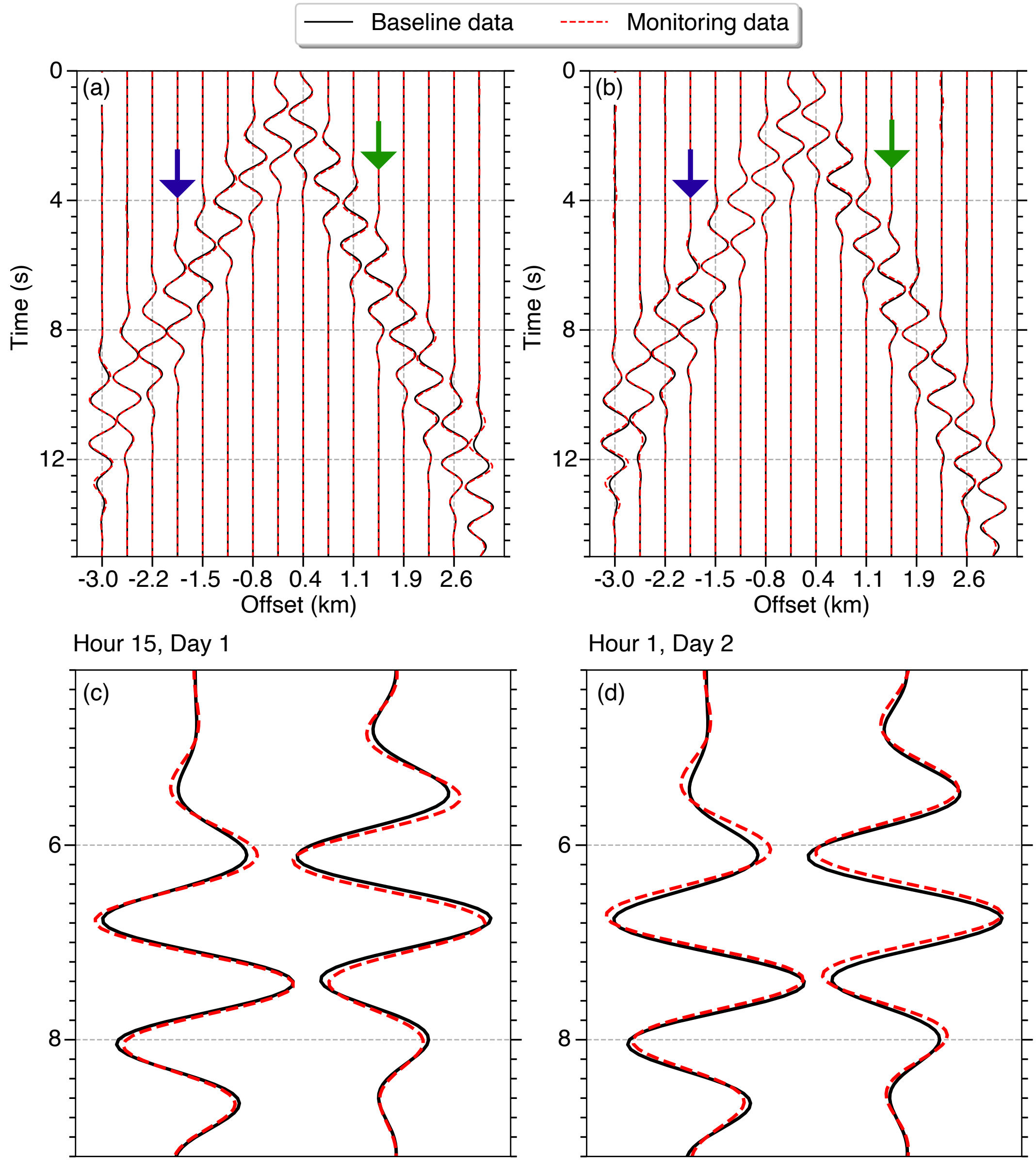

Figure 3. Common-station gathers sorted from CC functions of station pairs of Line 3924. (a) is the comparison of the reference data (solid black curve) and the monitoring data (dashed red curve) of Hour 15 Day 1. (b) is the comparison of the reference data (solid black curve) and the monitoring data (dashed red curve) of Hour 1 Day 2. (c) and (d) are closeups of the seismic traces at -1.9 km and 1.5 km offsets (from left to right, indicated by the blue and green arrows, respectively) from (a) and (b).

Previous studies have extensively utilized coda waves from ambient noise interferometry to monitor dv/v (e.g. Sens-Schönfelder & Wegler, 2006; Brenguier et al., 2008; Obermann, Schimmel, et al., 2013; Richter et al., 2014; Clements & Denolle, 2018; Takano et al., 2019). Multiply scattered wave propagation results in a more diffused noise wavefield than direct arrivals, making it less sensitive to the ambient noise source variations in time (Colombi et al., 2014; Mao et al., 2019). In contrast, the direct Scholte waves can exhibit greater sensitivity to the ambient noise source distribution and azimuthal variation over time (Weaver et al., 2009; Colombi et al., 2014; Takano et al., 2020). Therefore, it is crucial to verify that the observed waveform changes are from subsurface physical property changes, rather than being linked to variations in the ambient noise sources. We employ the beamforming method (Bucker, 1976; Bowden et al., 2021; Igel et al., 2023) to map the seafloor ambient noise source on an hourly basis. In order to maximize the potential resolution of the imaged source distribution of the incoming noise wavefield, we select the OBNs with a spiral-arm geometrical configuration (Figure 1c) (Kennett et al., 2015). Figure 4 displays the seafloor ambient noise sources during selected hours of Day 1, 2016. Throughout the monitoring periods, we observe consistent and stable ambient noise sources, with most of the energy concentrated in the south-east direction, parallel to the chosen line direction for cross correlation. The distribution of ambient noise source is consistent with the asymmetry in the cross-correlation functions (Figure 2). The mapped seafloor noise source has an apparent slowness of about 5 s/km (velocity of 0.2 km/s). Figure 5 shows the dominant azimuths of the incoming noise field during the two-day monitoring periods, calculated using the slowness vectors at the center-of-mass of the beamforming results, with a maximum perturbation of $\pm 1^\circ$ around an azimuth of 123° (from the north direction). Hence, we suggest that the seafloor ambient noise source during the entire monitoring period is stable. The observed time-lapse seismic velocity changes, derived from the extracted repetitive Scholte waves from seafloor ambient noise, are associated with time-lapse changes in the shear-wave velocity of the seafoor.

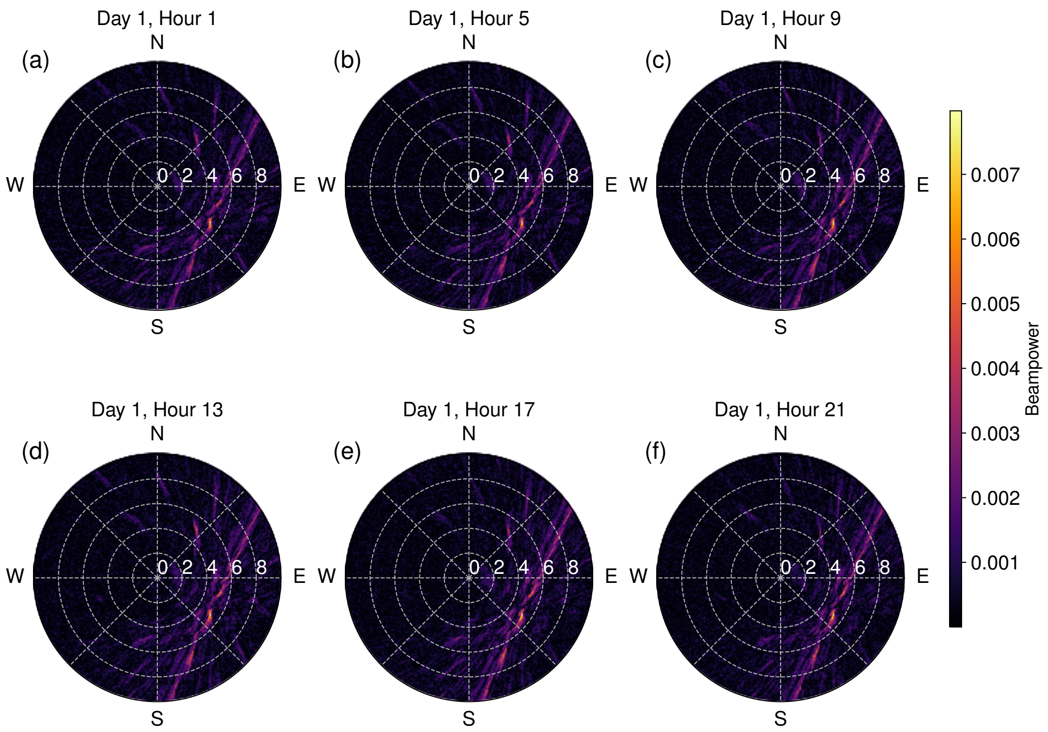

Figure 4. The beamforming images for mapping the ambient noise source distribution, from selected hours during the two-day passive monitoring period. The radial axis is the slowness (s/km) and the tangential axis denotes the azimuth angles. Warm colors suggest dominant ambient noise energy.

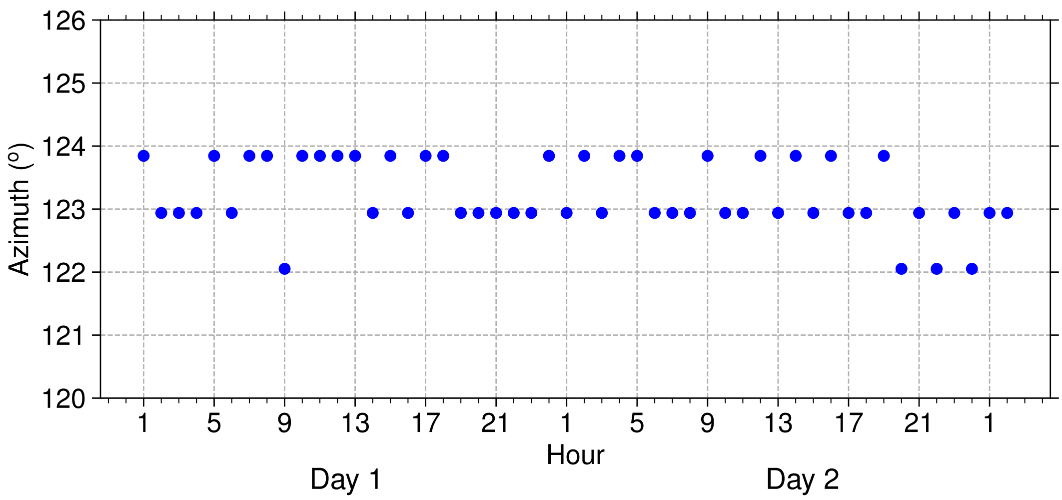

Figure 5. The dominant azimuths (from the north direction) of the ambient noise sources during the two-day passive monitoring period on an hourly basis.

3.2 High-resolution reference model estimation: full waveform inversion

The dense array of OBNs provides the opportunity for computing time-lapse quantitative images of seafloor velocity changes, i.e., localizing the temporal velocity changes in the subsurface in 2-D along node lines, from the continuous recordings of ambient noise using high-resolution waveform inversion technique.

A reference velocity model is necessary for estimating and comparing time-lapse subsurface models. We use the full waveform inversion (FWI) (Tarantola, 1984; Shipp & Singh, 2002; Guo et al., 2022) technique to estimate a high-resolution reference model using the extracted Scholte waves. In the numerical implementation, a gradient-based linearized inversion approach is used to update the velocity model iteratively with the aim of minimizing the misfit between synthetic and observed data, with the gradients of the data misfit to model parameters efficiently calculated by the adjoint-state method from the cross-correlation of the source and adjoint wavefields (Tarantola, 1984; Tromp et al., 2005; Fichtner et al., 2006). The source and adjoint wavefields can be obtained by source-wavelet generated forward wave propagation and adjoint-source generated backward wave propagation (Shipp & Singh, 2002). We use time-domain staggered-grid finite-difference with fourth-order spatial and second-order temporal accuracy to solve the elastic-wave equation in stress and particle-velocity formulation (Virieux, 1986). The grid spacing for the finite-difference was 25 m. A Gaussian smoothing operator with 200 m horizontal and 50 m vertical lengths was applied to the gradient for regularization.

We use the reference data in the form of common-station gathers (e.g., Figure 3) as the observed data for the reference FWI. Considering that the phase information in the virtual Scholte waves of the CC functions is more reliable than the amplitude, we employ a trace-normalized FWI method (Shen, 2010), with the misfit function J:

$$J = \sum_{i=1}^{\mathrm{Ns}} \sum_{j=1}^{\mathrm{Nr}} \| \frac{\mathbf{s}_{i,j}}{\|\mathbf{s}_{i,j}\|} - \frac{\mathbf{d}_{i,j}}{\|\mathbf{d}_{i,j}\|} \|^2, \tag{1}$$

where $\mathbf{s}_{i,j}$ and $\mathbf{d}_{i,j}$ are seismic traces (1-D time-series vectors) from the synthetic and field data respectively, $\| \; \|$ is the L-2 norm, i and j are the indexes for the sources and receivers, Ns and Nr are the number of sources and receivers.

The associated adjoint source that is used for adjoint wavefield propagation is

$$J = (\frac{\delta \mathbf{d}_{i,j}}{\|\mathbf{s}_{i,j}\|}) - (\frac{\delta \mathbf{d}_{i,j}^T \cdot \mathbf{d}_{i,j}}{\|\mathbf{s}_{i,j}\|^2} \frac{\mathbf{s}_{i,j}}{\|\mathbf{s}_{i,j}\|}), \tag{2}$$

where $\delta \mathbf{d}_{i,j} = \mathbf{s}_{i,j} - \mathbf{d}_{i,j}$ and T is the transpose operator.

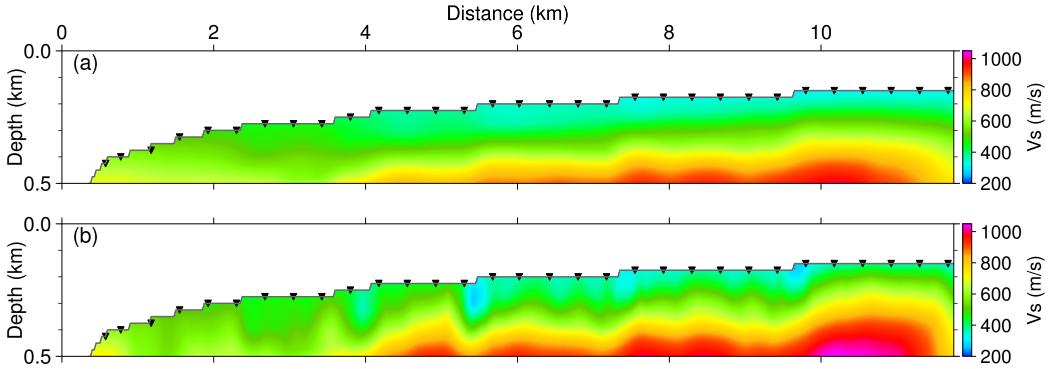

Figure 6. Shear-wave velocity models of the shallow seafloor. (a) Velocity model estimated from wave-equation dispersion inversion (Chen & Saygin, 2022); (b) velocity model estimated from the trace-normalized FWI method, using (a) as the starting model. The black triangles in (a) indicate the OBNs, with a spacing of ∼300 m.

Figure 6a shows the shear-velocity model from the wave-equation dispersion inversion, which uses the adjoint-state method for fitting the surface wave dispersion spectra (Li et al., 2017; Chen & Saygin, 2022). With the model in Figure 6a as the starting model, Figure 6b shows the velocity model obtained from the reference inversion using trace-normalized FWI after 50 iterations. The data misfit has been reduced significantly after FWI (Figure S4). The synthetic data after the FWI show a much better match (Figure S5) to the reference Scholte wave arrivals than those from the original tomographic model (Figure 6a). The velocity model in Figure 6b is used as the reference model for computing time-lapse seafloor models in the next section.

3.3 Localizing time-lapse velocity changes: wave-equation double-difference inversion

The most straightforward approach for extending seismic inversion to time-lapse monitoring entails conducting separate inversions for the reference and monitoring data. However, seismic inversion is usually a highly nonlinear problem, especially in the context of FWI (Tarantola, 1984; Shipp & Singh, 2002; Guo et al., 2021). The convergence level of seismic inversion of individual data can be different, as a result the model difference introduced by different local minima in successive inversions may generate misleading time-lapse subsurface models (Yang et al., 2016). In contrast, double-difference waveform inversion (DD-WI) (Denli & Huang, 2009; Zheng et al., 2011) directly inverts for the difference between reference and monitoring waveform data. This approach has been demonstrated for enhancing the reliability of time-lapse subsurface velocity models, with case studies utilizing body waves from controlled active seismic sources for imaging velocities changes (Yang et al., 2016; Zhou & Lumley, 2021).

Analysis of the ambient noise sources throughout the monitoring period indicates that the observed time-lapse changes stem from alterations in subsurface properties rather than temporal variations in the ambient noise source. The time-lapse difference of the extracted Scholte waves mainly manifests in variations of travel times (Figure 3). This observation implies that an objective function for the seismic time-lapse inversion problem using arrival time differences (shifts) between the monitoring and reference data may be more suitable for quantifying the time-lapse velocity models than including the complete waveform details in the inversion. Elastic wave equation based double-difference inversion (EW-DD) using travel time differences as an objective function has been proposed before, but in the context of seismic adjoint tomography for estimating seismic wave velocity structures, where the differential measurements are constructed between receivers (Yuan et al., 2016). We introduce this approach for time-lapse inversion based on elastic wave equation, where the differential measurements are constructed between reference and monitoring data.

Here, we propose the EW-DD method using travel time differences of the direct Scholte waves to obtain time-lapse velocity models using the extracted Scholte waves from ambient noise. The misfit function is defined as

$$J = \sum_{i=1}^{Ns} \sum_{j=1}^{Nr} \| \Delta t_{i,j}^{d} - \Delta t_{i,j}^{s} \|^2, \tag{3}$$

where $\Delta t_{(i,j)}^{d}$ is the travel time difference between the monitoring and the reference observed data, and $\Delta t_{(i,j)}^{s}$ is the travel time difference between the synthetic data from the monitoring model and the reference FWI model. i and j are the indexes for the sources and receivers, Ns and Nr are the number of sources and receivers. The time difference (shift) can be estimated by comparing waveform data using cross correlation. The term 'double-difference' comes from the two-level differences in equation 3: (1) the difference between reference and monitoring data, either synthetic or observed, and (2) the difference between the synthetic and observed measurements from (1).

The adjoint source for the EW-DD of travel time differences (Yuan et al., 2016), which is used for elastic wave propagation in backward time steps for computing the adjoint wavefields, can be derived as

$$\chi_{i,j} = (\Delta t_{i,j}^{d} - \Delta t_{i,j}^{s}) \partial_t \mathbf{s}_{i,j}(t - \Delta t_{i,j}^{s}), \tag{4}$$

where $s_{i,j}$ is a seismic waveform trace (1-D time-series vector) from the synthetic data. The only difference with the DD-WI is the adjoint source. Both the reference and time-lapse inversion methods honor the seafloor bathymetry which is implicitly included when solving the elastic-wave equation.

We apply the EW-DD method to differential measurements of monitoring and reference data to localize the shear-wave velocity changes in the seafloor on an hourly basis. We use the same inversion parameters, as described in the previous section for reference waveform inversion, in the time-lapse inversion. The misfit has been significantly reduced after the inversion (Figure S6). Figure 7 shows the time-lapse velocity difference between the reference model and the velocity models of selected hours at Day 1 and 2, in the horizontal and depth domain. The changes in Figure 7b and 7c are overall negative suggesting a slower velocity than the reference model, while the velocity changes in the remaining panels of Figure 7 are mainly positive indicating a faster velocity than the reference. The inferred negative/positive patterns in space are in agreement with Figures 2 and 3. The changes are more noticeable in Figure 7c than those in Figure 7b, consistent with Figure 2 (also Figure S7). We also apply the inversion method to the monitoring data from further survey lines (Figures S9, S10); the localized time-lapse velocity changes of the seafloor show consistent increasing/decreasing patterns with Figure S2.

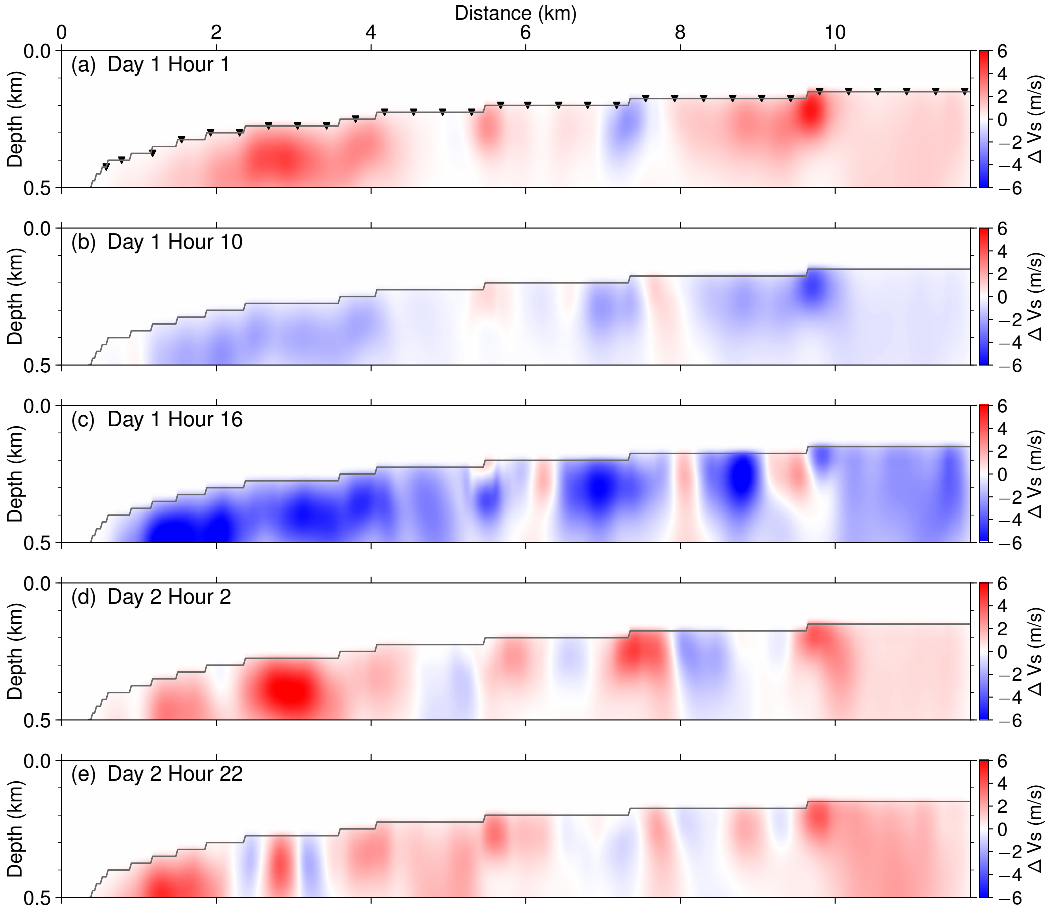

Figure 7. Time-lapse subsurface models of velocity changes compared with the reference model (Figure 6b), from selected hours during the two-day monitorig period. The black triangles in (a) indicate the locations of OBNs.

3.4 Resolution analysis of double-difference inversion using Scholte waves

The observed temporal velocity changes are subtle, especially when compared with the likely difference between the reference model from FWI and the ground truth of the seafloor. It is important to verify if these velocity changes are real, not artifacts coming from unfitted data in the reference inversion. Therefore we perform a series of synthetic tests, including errors in the reference model and noise in the reference and time-lapse data. We use the same frequency range, recording geometry and inversion parameters of the field data for these tests. The model in Figure 6b is used as the 'true' reference model for generating the 'observed' reference data. We then add 1% positive and negative Gaussian-shaped velocity anomalies ('time-lapse velocity changes', with 1 km horizontal extent and 0.2 km thickness, Figure 8a) to the reference model (Figure 6b) to generate the 'observed' monitoring data. We then add noise to the reference and monitoring data, respectively, so that the signal to noise ratio (S/N) is $\sim$8, lower than that of the extracted hourly CC functions (Figure 1c). The tomographic velocity model in Figure 6a, which contains much larger difference with the 'true' reference model than the added velocity anomalies, is then used as the starting model for the DD inversion. The recovered velocity changes are shown in Figure 8e. We also apply the same inversion workflow to velocity anomalies with a lower magnitude (0.5%, Figures 8b) and anomalies of different sizes (Figures 8c and 8d), with the inversion results shown in Figures 8f-

8h, respectively. In Figures 8c and 8d where the anomalies are smaller, the estimated anomalies (Figures 8g and 8h) from the DD inversion still provide a favorable match to the true model, although their features are relatively less well constrained. The data also has less resolution for the anomalies in the deeper part of the model (Figure 8g). The anomalies are better constrained in the horizontal direction than in the vertical diredtions, because the Scholte waves dominantly propagate along the seabed interface. The inversion results suggest that the proposed method is robust to errors in the reference model and data noise. The data can resolve subtle velocity changes on the scale of 0.5-1 km laterally, and ∼200 m vertically.

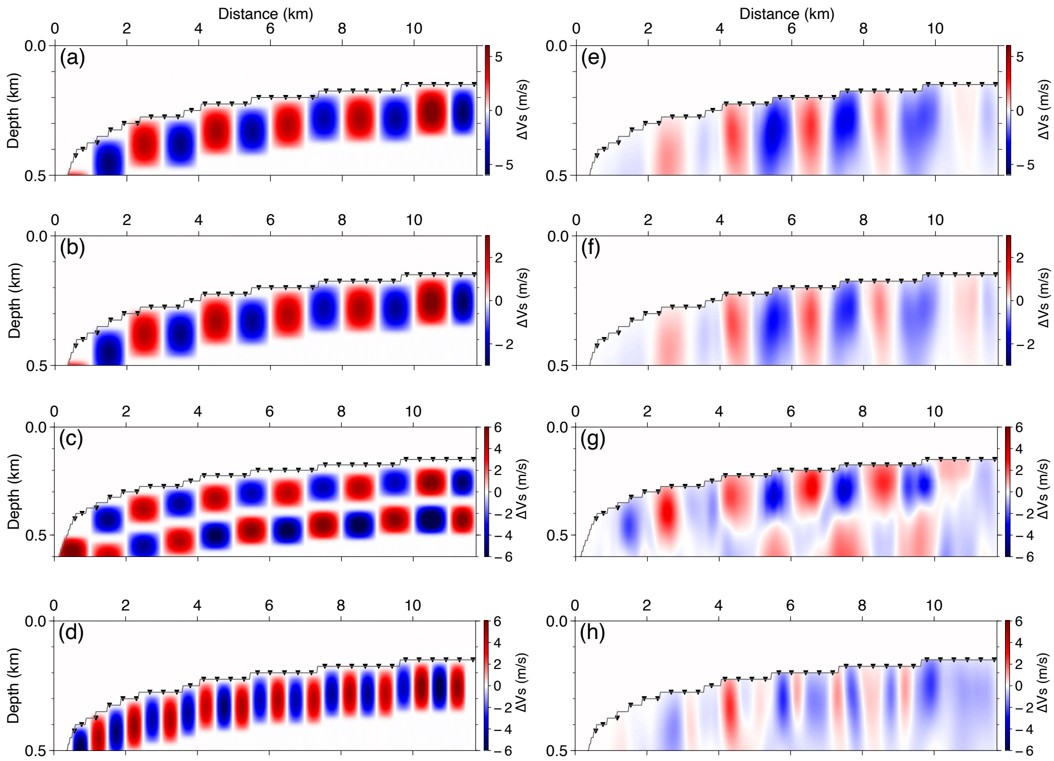

Figure 8. Checkerboard test for time-lapse wave-equation double-difference inversion. The velocity anomalies (time-lapse velocity changes) in (a) have a size of 1 km and 0.2 km horizontally and vertically, respectively, with magnitude of 1%, (b) have the same size but magnitude of 0.5%, (c) have a size of 1 km and 0.1 km horizontally and vertically, and (d) have a size of 0.5 km and 0.2 km horizontally and vertically. (e)-(h) show the recovered velocity anomalies from time-lapse inversion using Scholte waves. The black triangles at the seafloor indicate the locations of OBNs.

4 Discussion

The phenomenon of temporal variation in seismic velocity is ubiquitous and has been associated with different physical mechanisms. For example, both velocity increase (Wegler et al., 2006; Yates et al., 2019) and decrease (Brenguier et al., 2008; Obermann, Schimmel, et al., 2013) have been observed before the eruption of volcanos, indicating distinct deformational styles depending on the position of the pressure source (Yates et al., 2019). On the other hand, velocity changes with a periodic pattern tend to be related to environmental factors, such as climatic perturbations including temperature (Richter et al., 2014; Sens-Schönfelder & Eulenfeld, 2019) and precipitation (Sens-Schönfelder & Wegler, 2006; Oakley et al., 2021; Mao et al., 2022), and the gravitational field of the Sun and Moon resulting in tidal deformation, comprising of solid earth tide and ocean tide loading (De Fazio et al., 1973; Yamamura et al., 2003; Hillers et al., 2015; Takano & Nishida, 2023). Such perturbations cause strain changes in the subsurface rock, leading to the changes in the velocity of the seismic waves. In recent years, emerging monitoring techniques using seismic ambient noise allow continuous and real-time monitoring of seismic velocity variations in a cost-effective and eco-friendly way (Sens-Schönfelder & Wegler, 2006; Donaldson et al., 2017). Takano et al. (2014) revealed onshore seismic shear-wave velocity decrease of 0.1-0.3% caused by solid earth tide during crustal dilatation compared with that from the contraction episodes. The opening and closure of cracks or pores in rocks induced by strain changes lead to velocity decrease and increase, respectively (Yamamura et al., 2003; Takano et al., 2014). Mao et al. (2019) presented seismic velocity monitoring with hourly temporal resolution using a dense array of seismometers and suggest that the diurnal dv/v changes are likely induced by a superposition of tidal and thermal effects. The tidal-induced velocity changes are usually constrained to the shallow crust (Hillers et al., 2015). Moreover, large temporal velocity changes up to 1% (Takano & Nishida, 2023) have been observed in the low shear-wave velocity region of the shallow crust using hourly stacked ambient noise auto-correlations, which have been associated with the solid earth tide. Notably, this study suggests that the response of seismic velocity to strain changes becomes more sensitive when the shear-wave velocity is low (Takano & Nishida, 2023), resulting in increasing relative velocity changes with decreasing shear-wave velocity. The strain-velocity sensitivity varies from approximately 10^3 to 10^5 in Takano and Nishida (2023). This could explain the observed much smaller velolocity changes induced by tidal deformation from previous studies, for example, the magnitude of dv/v is about 0.08% at the Piton de la Fournaise volcano, where the subsurface velocity is higher than that of the sedimentary layers (Mordret et al., 2015). In addition, recent studies also revealed periodic seismic velocity variations at the order of 0.01% associated with atmosphereic pressure changes (Gradon et al., 2021; Kramer et al., 2023).

Studies for time-lapse seafloor seismic velocity are relatively rare compared with those of the continental (onshore) crust. We observe up to 0.8% shear-wave velocity change in the seafloor, which contains thick sediments with low shear-wave velocities (Figure 6) and as a result high strain-velocity sensitivity (Takano & Nishida, 2023). Figure 9 shows the comparison of the time-lapse velocity changes with the variations of the sea level height measured on a pressure inverted echo sounder about 8 km away. The velocity exhibits an inversely correlation with the sea level height, i.e., the velocity decreases with increasing sea level. This observation contradicts the expectation that increasing confining stress (e.g. higher sea level) results in the closing of cracks or pores in the subsurface, which leads to an increase in seismic velocity (Takano et al., 2014). Hillers et al. (2015) observed similar phenomenon from onshore vertical component coda waves, that the velocity of seismic waves reduces during periods of volumetric compression induced by solid earth tide loading. This seemingly surprising decrease in velocity with increasing confining stress is indeed compatible with previous resonant bar experiments using relatively porous, compliant rock samples characterized by very low seismic velocities (Zinszner et al., 1997; Pasqualini et al., 2007). The porous seafloor with low seismic velocities here could be comparable to the onshore shallow crust with weathered, almost totally decomposed granodiorite which grades into grus and corestones near the San Jacinto Fault in Hillers et al. (2015). The porous, low velocity material can experience dilatancy from inelastic damage under compression, resulting in decreasing seismic velocities, which implies a different response to cyclic deformation compared to more compact, solidified rocks (Zinszner et al., 1997; Pasqualini et al., 2007). Moreover, using active-source seismic experiments with piezoelectric transducer as the source, Yamamura et al. (2003) found diurnal variations in the inland seismic velocity with an amplitude of 0.3% about 20 m from the coast, which also anti-correlates in pattern and phase with the in-situ areal strain and sea level heights, while the role of the solid earth tide is negligible. Other recent studies show reduced seismic velocity in a sea levee (Planès et al., 2017) and a sea dike (Joubert et al., 2018) when the sea level is high. The underlying mechanism involves infiltrated water at high sea levels raising in-situ pore-water pressure, which subsequently reduces effective stress and shear-wave velocity (Planès et al., 2017; Joubert et al., 2018). Kramer et al. (2023) suggest that in saturated conditions (e.g. at the seafloor), when cracks close from increasing stress, the fluid within is pushed to the pores, which leads to an overall increase of the pore pressure and a decrease of seismic velocity. Furthermore, Andajani et al. (2022) found that the correlation between sea level height and nearby inland seismic velocity changes can be negative or positive, depending on the in-situ local stress, orientation of dominant crack, and hydraulic conductivity. The local heterogeneities (Andajani et al., 2022) in the seafloor could also be the reason for the observed negative anomalies in the time-lapse seafloor images (Figure 7) associated with positive velocity changes and the positive anomalies in the images corresponding to negative velocity changes, although we acknowledge that some of the anomalies could also beyond the resolution of seismic inversion. Taken together, the time-lapse velocity variations in the seafloor could be related to dilatant effects for porous, low velocity shallow seafloor and the pore pressure changes associated with sea level. We also acknowledge that the short passive monitoring period of two days, limited by the data acquisition in this study, hinder a complete and comprehensive study of the seafloor property time-lapse changes with environmental factors such as sea level heights. Future studies should use at least a few months of data (Yamamura et al., 2003).

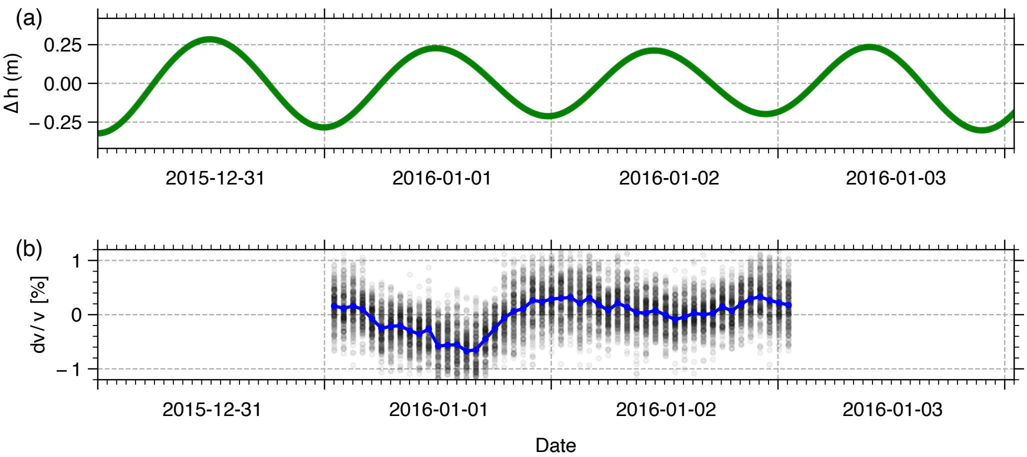

Figure 9. A comparison of (a) the sea level heights and (b) the time-lapse relative seismic velocity changes (dv/v). (a) was measured using a pressure inverted echo sounder about 8 km away from the survey line 3924, then zero-phase bandpass filtered around 1 cycle per day. (b) is the same with Figure 2c.

5 Conclusion

In this study, we propose a passive space-time monitoring technique for real-time tracking of subsurface property changes with high temporal (hourly) and spatial (hundreds of meters) resolution. Using seismic ambient noise data recorded by a dense array of ocean bottom nodes offshore Western Australia, we detect temporal variations of shear-wave velocity of up to 0.8% in the seafloor, with a likely 24-hour cycling pattern.

The velocity seems inversely correlated with sea level height, decreasing with increasing sea level, possibly associated with dilatant effects for porous, low-velocity shallow seafloor and rising pore pressure with high sea level. To localize the velocity changes in the subsurface, we first build a high-resolution reference seafloor model from FWI of Scholte waves. Then using the double difference of arrival time differences between reference and monitoring data, we obtain quantitative time-lapse seafloor images in the horizontal and depth domain containing the heterogeneous relative velocity variations. The elastic-wave equation based workflow from building a high-resolution reference model to time-lapse inversion using Scholte wave measurements honors the full wave physics, is robust to data noise and errors from the reference model, and is sensitive to subtle velocity changes. A comparable approach can be applied to passive seismic data from dense seismic arrays and Distributed Acoustic Sensing (DAS) for real-time monitoring of groundwater level, volcano, subduction zone and CO_2 capture storage, in the aim for an in-depth understanding of the evolving 4-D Earth.

Open Research Section

The data used for reproducing the figures, including the hourly CC functions, dv/v measurements and seismic velocity models, are publicly available at https://doi.org/10.5281/zenodo.6804990.

Acknowledgments

This research was funded by the Deep Earth Imaging Future Science Platform, CSIRO. This work was supported by resources provided by the Pawsey Supercomputing Centre with funding from the Australian Government and the Government of Western Australia. The raw seismic data of the Gorgon Ocean Bottom Node Seismic Survey (ID: ENO0603054) can be requested from the National Offshore Petroleum Information Management System (NOPIMS) via contacting AusGeoData@ga.gov.au. We thank Chevron Australia for their assistance with the data.

References

Andajani, R. D., Tsuji, T., Snieder, R., & Ikeda, T. (2022). Spatial and temporal influence of sea level on inland stress based on seismic velocity monitoring. *Earth, Planets and Space*, *74*(1), 97.

Ardhuin, F., Gualtieri, L., & Stutzmann, E. (2015). How ocean waves rock the Earth: Two mechanisms explain microseisms with periods 3 to 300 s. *Geophysical Research Letters*, *42*(3), 765–772.

Arts, R., Eiken, O., Chadwick, A., Zweigel, P., Van Der Meer, B., & Kirby, G. (2004). Seismic monitoring at the Sleipner underground CO2 storage site (North Sea). *Geological Society, London, Special Publications*, *233*(1), 181–191.

Barreyre, T., Parnell-Turner, R., Wu, J.-N., & Fornari, D. (2022). Tracking crustal permeability and hydrothermal response during seafloor eruptions at the East Pacific Rise, 9 50'N. *Geophysical Research Letters*, *49*(3), e2021GL095459.

Batzle, M., & Wang, Z. (1992). Seismic properties of pore fluids. *Geophysics*, *57*(11), 1396–1408.

Bensen, G., Ritzwoller, M., Barmin, M., Levshin, A. L., Lin, F., Moschetti, M., ... Yang, Y. (2007). Processing seismic ambient noise data to obtain reliable broad-band surface wave dispersion measurements. *Geophysical journal international*, *169*(3), 1239–1260.

Bowden, D. C., Sager, K., Fichtner, A., & Chmiel, M. (2021). Connecting beamforming and kernel-based noise source inversion. *Geophysical Journal International*, *224*(3), 1607–1620.

Brenguier, F., Campillo, M., Takeda, T., Aoki, Y., Shapiro, N., Briand, X., ...

Miyake, H. (2014). Mapping pressurized volcanic fluids from induced crustal seismic velocity drops. *Science*, *345*(6192), 80–82.

Brenguier, F., Courbis, R., Mordret, A., Campman, X., Boué, P., Chmiel, M., ... others (2020). Noise-based ballistic wave passive seismic monitoring. part 1: body waves. *Geophysical Journal International*, *221*(1), 683–691.

Brenguier, F., Rivet, D., Obermann, A., Nakata, N., Boué, P., Lecocq, T., ... Shapiro, N. (2016). 4-D noise-based seismology at volcanoes: Ongoing efforts and perspectives. *Journal of Volcanology and Geothermal Research*, *321*, 182–195.

Brenguier, F., Shapiro, N. M., Campillo, M., Ferrazzini, V., Duputel, Z., Coutant, O., & Nercessian, A. (2008). Towards forecasting volcanic eruptions using seismic noise. *Nature Geoscience*, *1*(2), 126–130.

Bucker, H. P. (1976). Use of calculated sound fields and matched-field detection to locate sound sources in shallow water. *The Journal of the Acoustical Society of America*, *59*(2), 368–373.

Campillo, M., & Paul, A. (2003). Long-range correlations in the diffuse seismic coda. *Science*, *299*(5606), 547–549.

Castellanos, J. C., Clayton, R. W., & Juarez, A. (2020). Using a time-based subarray method to extract and invert noise-derived body waves at Long Beach, California. *Journal of Geophysical Research: Solid Earth*, *125*(5), e2019JB018855.

Chen, Y., & Saygin, E. (2022). 3D S wave imaging via robust neural network interpolation of 2D profiles from wave equation dispersion inversion of seismic ambient noise. *Journal of Geophysical Research: Solid Earth*, e2022JB024663.

Clarke, D., Zaccarelli, L., Shapiro, N., & Brenguier, F. (2011). Assessment of resolution and accuracy of the Moving Window Cross Spectral technique for monitoring crustal temporal variations using ambient seismic noise. *Geophysical Journal International*, *186*(2), 867–882.

Clements, T., & Denolle, M. A. (2018). Tracking groundwater levels using the ambient seismic field. *Geophysical Research Letters*, *45*(13), 6459–6465.

Colombi, A., Chaput, J., Brenguier, F., Hillers, G., Roux, P., & Campillo, M. (2014). On the temporal stability of the coda of ambient noise correlations. *Comptes Rendus Geoscience*, *346*(11-12), 307–316.

De Fazio, T. L., Aki, K., & Alba, J. (1973). Solid earth tide and observed change in the in situ seismic velocity. *Journal of Geophysical Research*, *78*(8), 1319–1322.

Denli, H., & Huang, L. (2009). Double-difference elastic waveform tomography in the time domain. In *2009 seg annual meeting.*

de Ridder, S., & Biondi, B. (2013). Daily reservoir-scale subsurface monitoring using ambient seismic noise. *Geophysical Research Letters*, *40*(12), 2969–2974.

de Ridder, S., Biondi, B., & Clapp, R. (2014). Time-lapse seismic noise correlation tomography at Valhall. *Geophysical Research Letters*, *41*(17), 6116–6122.

Donaldson, C., Caudron, C., Green, R. G., Thelen, W. A., & White, R. S. (2017). Relative seismic velocity variations correlate with deformation at Kīlauea volcano. *Science advances*, *3*(6), e1700219.

Fichtner, A., Bunge, H.-P., & Igel, H. (2006). The adjoint method in seismology: I. theory. *Physics of the Earth and Planetary Interiors*, *157*(1-2), 86–104.

Fokker, E., Ruigrok, E., Hawkins, R., & Trampert, J. (2023). 4D physics-based pore pressure monitoring using passive image interferometry. *Geophysical Research Letters*, *50*(5), e2022GL101254.

Gradon, C., Brenguier, F., Stammeijer, J., Mordret, A., Hindriks, K., Campman, X., ... Chmiel, M. (2021). Seismic velocity response to atmospheric pressure using time-lapse passive seismic interferometry. *Bulletin of the Seismological Society of America*, *111*(6), 3451–3458.

Gualtieri, L., Bachmann, E., Simons, F. J., & Tromp, J. (2020). The origin of secondary microseism Love waves. *Proceedings of the National Academy of Sciences*, *117*(47), 29504–29511.

Guo, P., Singh, S., Vaddineni, V., Grevemeyer, I., & Saygin, E. (2022). Lower oceanic crust formed by in situ melt crystallization revealed by seismic layering. *Nature Geoscience*, *15*, 591–596.

Guo, P., Singh, S. C., Vaddineni, V. A., Visser, G., Grevemeyer, I., & Saygin, E. (2021). Nonlinear full waveform inversion of wide-aperture OBS data for Moho structure using a trans-dimensional bayesian method. *Geophysical Journal International*, *224*(2), 1056–1078.

Hadziioannou, C., Larose, E., Baig, A., Roux, P., & Campillo, M. (2011). Improving temporal resolution in ambient noise monitoring of seismic wave speed. *Journal of Geophysical Research: Solid Earth*, *116*(B7).

Hasselmann, K. (1963). A statistical analysis of the generation of microseisms. *Reviews of Geophysics*, *1*(2), 177–210.

Hicks, E., Hoeber, H., Houbiers, M., Lescoffit, S. P., Ratcliffe, A., & Vinje, V. (2016). Time-lapse full-waveform inversion as a reservoir-monitoring tool—a North Sea case study. *The Leading Edge*, *35*(10), 850–858.

Hillers, G., Retailleau, L., Campillo, M., Inbal, A., Ampuero, J.-P., & Nishimura, T. (2015). In situ observations of velocity changes in response to tidal deformation from analysis of the high-frequency ambient wavefield. *Journal of Geophysical Research: Solid Earth*, *120*(1), 210–225.

Igel, J. K., Bowden, D. C., & Fichtner, A. (2023). SANS: Publicly available daily multi-scale seismic ambient noise source maps. *Journal of Geophysical Research: Solid Earth*, *128*(1), e2022JB025114.

Joubert, A., Le Feuvre, M., & Côte, P. (2018). Passive monitoring of a sea dike during a tidal cycle using sea waves as a seismic noise source. *Geophysical Journal International*, *214*(2), 1364–1378.

Kamei, R., & Lumley, D. (2017). Full waveform inversion of repeating seismic events to estimate time-lapse velocity changes. *Geophysical Journal International*, *209*(2), 1239–1264.

Kennett, B., Stipčević, J., & Gorbatov, A. (2015). Spiral-arm seismic arrays. *Bulletin of the Seismological Society of America*, *105*(4), 2109–2116.

Kramer, R., Lu, Y., & Bokelmann, G. (2023). Interaction of air pressure and groundwater as main cause of sub-daily relative seismic velocity changes. *Geophysical Research Letters*, *50*(7), e2022GL101298.

Krevor, S., De Coninck, H., Gasda, S. E., Ghaleigh, N. S., de Gooyert, V., Hajibeygi, H., ... Swennenhuis, F. (2023). Subsurface carbon dioxide and hydrogen storage for a sustainable energy future. *Nature Reviews Earth & Environment*, *4*(2), 102–118.

Larose, E., Margerin, L., Derode, A., van Tiggelen, B., Campillo, M., Shapiro, N., ... Tanter, M. (2006). Correlation of random wavefields: An interdisciplinary review. *Geophysics*, *71*(4), SI11–SI21.

Lecocq, T., Caudron, C., & Brenguier, F. (2014). MSNoise, a python package for monitoring seismic velocity changes using ambient seismic noise. *Seismological Research Letters*, *85*(3), 715–726.

Li, J., Feng, Z., & Schuster, G. (2017). Wave-equation dispersion inversion. *Geophysical Journal International*, *208*(3), 1567–1578.

Lindsey, N. J., Dawe, T. C., & Ajo-Franklin, J. B. (2019). Illuminating seafloor faults and ocean dynamics with dark fiber distributed acoustic sensing. *Science*, *366*(6469), 1103–1107.

Longuet-Higgins, M. S. (1950). A theory of the origin of microseisms. *Philosophical Transactions of the Royal Society of London. Series A, Mathematical and Physical Sciences*, *243*(857), 1–35.

Lumley, D. (2001). Time-lapse seismic reservoir monitoring. *Geophysics*, *66*(1), 50–53.

Lumley, D. (2010). 4D seismic monitoring of CO2 sequestration. *The Leading Edge*, *29*(2), 150–155.

Mao, S., Campillo, M., van Der Hilst, R. D., Brenguier, F., Stehly, L., & Hillers, G. (2019). High temporal resolution monitoring of small variations in crustal strain by dense seismic arrays. *Geophysical Research Letters*, *46*(1), 128–137.

Mao, S., Ellsworth, W. L., & Beroza, G. C. (2023). Adaptive coda-wave imaging with voronoi tessellation. *Journal of Geophysical Research: Solid Earth*, *128*(8), e2023JB026592.

Mao, S., Lecointre, A., van der Hilst, R. D., & Campillo, M. (2022). Space-time monitoring of groundwater fluctuations with passive seismic interferometry. *Nature communications*, *13*(1), 4643.

Margerin, L., Planès, T., Mayor, J., & Calvet, M. (2016). Sensitivity kernels for coda-wave interferometry and scattering tomography: theory and numerical evaluation in two-dimensional anisotropically scattering media. *Geophysical Journal International*, *204*(1), 650–666.

Minato, S., Tsuji, T., Ohmi, S., & Matsuoka, T. (2012). Monitoring seismic velocity change caused by the 2011 Tohoku-oki earthquake using ambient noise records. *Geophysical Research Letters*, *39*(9).

Mordret, A., Courbis, R., Brenguier, F., Chmiel, M., Garambois, S., Mao, S., ... others (2020). Noise-based ballistic wave passive seismic monitoring–part 2: surface waves. *Geophysical Journal International*, *221*(1), 692–705.

Mordret, A., Rivet, D., Landès, M., & Shapiro, N. M. (2015). Three-dimensional shear velocity anisotropic model of Piton de la Fournaise Volcano (la réunion island) from ambient seismic noise. *Journal of Geophysical Research: Solid Earth*, *120*(1), 406–427.

Mordret, A., Shapiro, N. M., & Singh, S. (2014). Seismic noise-based time-lapse monitoring of the Valhall overburden. *Geophysical Research Letters*, *41*(14), 4945–4952.

Nakata, N., Boué, P., Brenguier, F., Roux, P., Ferrazzini, V., & Campillo, M. (2016). Body and surface wave reconstruction from seismic noise correlations between arrays at Piton de la Fournaise volcano. *Geophysical Research Letters*, *43*(3), 1047–1054.

Nishida, K. (2013). Earth's background free oscillations. *Annual Review of Earth and Planetary Sciences*, *41*, 719–740.

Oakley, D. O., Forsythe, B., Gu, X., Nyblade, A. A., & Brantley, S. L. (2021). Seismic ambient noise analyses reveal changing temperature and water signals to 10s of meters depth in the critical zone. *Journal of Geophysical Research: Earth Surface*, *126*(2), e2020JF005823.

Obermann, A., Kraft, T., Larose, E., & Wiemer, S. (2015). Potential of ambient seismic noise techniques to monitor the St. Gallen geothermal site (Switzerland). *Journal of Geophysical Research: Solid Earth*, *120*(6), 4301–4316.

Obermann, A., Planès, T., Larose, E., Sens-Schönfelder, C., & Campillo, M. (2013). Depth sensitivity of seismic coda waves to velocity perturbations in an elastic heterogeneous medium. *Geophysical Journal International*, *194*(1), 372–382.

Obermann, A., Schimmel, M., Weemstra, C., Verdel, A., & Jousset, P. (2013). Imaging preeruptive and coeruptive structural and mechanical changes of a volcano with ambient seismic noise. *Journal of Geophysical Research: Solid Earth*, *118*(12), 6285–6294.

Pacheco, C., & Snieder, R. (2005). Time-lapse travel time change of multiply scattered acoustic waves. *The Journal of the Acoustical Society of America*, *118*(3), 1300–1310.

Pasqualini, D., Heitmann, K., TenCate, J. A., Habib, S., Higdon, D., & Johnson, P. A. (2007). Nonequilibrium and nonlinear dynamics in Berea and Fontainebleau sandstones: Low-strain regime. *Journal of Geophysical Research: Solid Earth*, *112*(B1).

Planès, T., Rittgers, J. B., Mooney, M. A., Kanning, W., & Draganov, D. (2017). Monitoring the tidal response of a sea levee with ambient seismic noise. *Journal of Applied Geophysics*, *138*, 255–263.

Poupinet, G., Ellsworth, W., & Frechet, J. (1984). Monitoring velocity variations in the crust using earthquake doublets: An application to the Calaveras Fault, California. *Journal of Geophysical Research: Solid Earth*, *89*(B7), 5719–5731.

Rentsch, S., Thompson, J., Adams, R., Moore, D., & Raborn, R. (2023). 100 Ocean Bottom Nodes with their CSAC clock drift analysed for 91 days: three controlled experiments. In *84th eage annual conference & exhibition* (Vol. 2023, pp. 1–5).

Richter, T., Sens-Schönfelder, C., Kind, R., & Asch, G. (2014). Comprehensive observation and modeling of earthquake and temperature-related seismic velocity changes in northern Chile with passive image interferometry. *Journal of Geophysical Research: Solid Earth*, *119*(6), 4747–4765.

Ringrose, P. S., Furre, A.-K., Gilfillan, S. M., Krevor, S., Landrø, M., Leslie, R., ... Zahid, A. (2021). Storage of carbon dioxide in saline aquifers: Physicochemical processes, key constraints, and scale-up potential. *Annual Review of Chemical and Biomolecular Engineering*, *12*, 471–494.

Rodríguez Tribaldos, V., & Ajo-Franklin, J. B. (2021). Aquifer monitoring using ambient seismic noise recorded with distributed acoustic sensing DAS deployed on dark fiber. *Journal of Geophysical Research: Solid Earth*, *126*(4), e2020JB021004.

Roux, P., Sabra, K. G., Gerstoft, P., Kuperman, W., & Fehler, M. C. (2005). P-waves from cross-correlation of seismic noise. *Geophysical Research Letters*, *32*(19).

Sánchez-Pastor, P., Obermann, A., & Schimmel, M. (2018). Detecting and locating precursory signals during the 2011 El Hierro, Canary islands, submarine eruption. *Geophysical Research Letters*, *45*(19), 10–288.

Sánchez-Pastor, P., Obermann, A., Schimmel, M., Weemstra, C., Verdel, A., & Jousset, P. (2019). Short-and long-term variations in the reykjanes geothermal reservoir from seismic noise interferometry. *Geophysical Research Letters*, *46*(11), 5788–5798.

Saygin, E., Cummins, P. R., & Lumley, D. (2017). Retrieval of the P wave reflectivity response from autocorrelation of seismic noise: Jakarta Basin, Indonesia. *Geophysical Research Letters*, *44*(2), 792–799.

Saygin, E., & Kennett, B. (2012). Crustal structure of Australia from ambient seismic noise tomography. *Journal of Geophysical Research: Solid Earth*, *117*(B1).

Schimmel, M., Stutzmann, E., & Gallart, J. (2011). Using instantaneous phase coherence for signal extraction from ambient noise data at a local to a global scale. *Geophysical Journal International*, *184*(1), 494–506.

Sens-Schönfelder, C., & Eulenfeld, T. (2019). Probing the in situ elastic nonlinearity of rocks with earth tides and seismic noise. *Physical review letters*, *122*(13), 138501.

Sens-Schönfelder, C., & Wegler, U. (2006). Passive image interferometry and seasonal variations of seismic velocities at Merapi Volcano, Indonesia. *Geophysical research letters*, *33*(21).

Shapiro, N. M., & Campillo, M. (2004). Emergence of broadband Rayleigh waves from correlations of the ambient seismic noise. *Geophysical Research Letters*, *31*(7).

Shen, X. (2010). Near-surface velocity estimation by weighted early-arrival waveform inversion. In *2010 seg annual meeting.*

Shipp, R. M., & Singh, S. C. (2002). Two-dimensional full wavefield inversion of wide-aperture marine seismic streamer data. *Geophysical Journal International*, *151*(2), 325–344.

Snieder, R., Grêt, A., Douma, H., & Scales, J. (2002). Coda wave interferometry for estimating nonlinear behavior in seismic velocity. *Science*, *295*(5563), 2253–2255.
Stehly, L., Campillo, M., & Shapiro, N. (2006). A study of the seismic noise from its long-range correlation properties. *Journal of Geophysical Research: Solid Earth*, *111*(B10).
Takano, T., Brenguier, F., Campillo, M., Peltier, A., & Nishimura, T. (2020). Noise-based passive ballistic wave seismic monitoring on an active volcano. *Geophysical Journal International*, *220*(1), 501–507.
Takano, T., & Nishida, K. (2023). Tidal response of seismic wave velocity at shallow crust in Japan. *Geophysical Research Letters*, *50*(9), e2023GL103011.
Takano, T., Nishimura, T., Nakahara, H., Ohta, Y., & Tanaka, S. (2014). Seismic velocity changes caused by the Earth tide: Ambient noise correlation analyses of small-array data. *Geophysical Research Letters*, *41*(17), 6131–6136.
Takano, T., Nishimura, T., Nakahara, H., Ueda, H., & Fujita, E. (2019). Sensitivity of seismic velocity changes to the tidal strain at different lapse times: data analyses of a small seismic array at Izu-Oshima volcano. *Journal of Geophysical Research: Solid Earth*, *124*(3), 3011–3023.
Tarantola, A. (1984). Inversion of seismic reflection data in the acoustic approximation. *Geophysics*, *49*(8), 1259–1266.
Tonegawa, T., Takagi, R., Sawazaki, K., & Shiomi, K. (2023). Short-term and long-term variations in seismic velocity at shallow depths of the overriding plate west of the Japan trench. *Journal of Geophysical Research: Solid Earth*, *128*(1), e2022JB025262.
Tromp, J., Tape, C., & Liu, Q. (2005). Seismic tomography, adjoint methods, time reversal and banana-doughnut kernels. *Geophysical Journal International*, *160*(1), 195–216.
Viens, L., Denolle, M. A., Hirata, N., & Nakagawa, S. (2018). Complex near-surface rheology inferred from the response of greater Tokyo to strong ground motions. *Journal of Geophysical Research: Solid Earth*, *123*(7), 5710–5729.
Virieux, J. (1986). P-SV wave propagation in heterogeneous media: Velocity-stress finite-difference method. *Geophysics*, *51*(4), 889–901.
Weaver, R., Froment, B., & Campillo, M. (2009). On the correlation of non-isotropically distributed ballistic scalar diffuse waves. *The Journal of the Acoustical Society of America*, *126*(4), 1817–1826.
Wegler, U., Lühr, B.-G., Snieder, R., & Ratdomopurbo, A. (2006). Increase of shear wave velocity before the 1998 eruption of Merapi volcano (Indonesia). *Geophysical Research Letters*, *33*(9).
Yamamura, K., Sano, O., Utada, H., Takei, Y., Nakao, S., & Fukao, Y. (2003). Long-term observation of in situ seismic velocity and attenuation. *Journal of Geophysical Research: Solid Earth*, *108*(B6).
Yang, D., Liu, F., Morton, S., Malcolm, A., & Fehler, M. (2016). Time-lapse full-waveform inversion with ocean-bottom-cable data: Application on Valhall field. *Geophysics*, *81*(4), R225–R235.
Yates, A., Savage, M., Jolly, A., Caudron, C., & Hamling, I. (2019). Volcanic, coseismic, and seasonal changes detected at White Island (Whakaari) volcano, New Zealand, using seismic ambient noise. *Geophysical Research Letters*, *46*(1), 99–108.
Yuan, Y. O., Simons, F. J., & Tromp, J. (2016). Double-difference adjoint seismic tomography. *Geophysical Journal International*, *206*(3), 1599–1618.
Zhang, S., Luo, B., Ben-Zion, Y., Lumley, D. E., & Zhu, H. (2023). Monitoring terrestrial water storage, drought and seasonal changes in central Oklahoma with ambient seismic noise. *Geophysical Research Letters*, *50*(17), e2023GL103419.
Zhang, Z., & Huang, L. (2013). Double-difference elastic-waveform inversion with prior information for time-lapse monitoring. *Geophysics*, *78*(6), R259–R273.

Zheng, Y., Barton, P., & Singh, S. (2011). Strategies for elastic full waveform inversion of time-lapse ocean bottom cable (OBC) seismic data. In *Seg technical program expanded abstracts 2011* (pp. 4195–4200). Society of Exploration Geophysicists.

Zhou, W., & Lumley, D. (2021). Nonrepeatability effects on time-lapse 4D seismic full-waveform inversion for ocean-bottom node data. *Geophysics*, *86*(4), R547–R561.

Zhu, T., Ajo-Franklin, J., Daley, T. M., & Marone, C. (2019). Dynamics of geologic CO2 storage and plume motion revealed by seismic coda waves. *Proceedings of the National Academy of Sciences*, *116*(7), 2464–2469.

Zinszner, B., Johnson, P. A., & Rasolofosaon, P. N. (1997). Influence of change in physical state on elastic nonlinear response in rock: Significance of effective pressure and water saturation. *Journal of Geophysical Research: Solid Earth*, *102*(B4), 8105–8120.